INVITED PAPER

The underestimated impact of instabilities with nanoimprint

A. Mayer[1] · K. Dhima[1] · S. Wang[1] · C. Steinberg[1] · M. Papenheim[1] ·
H.-C. Scheer[1]

Abstract   With nanoimprint, instabilities of the polymeric
layer between the substrate and the stamp are observed
when incomplete filling of the stamp cavities prevails,
resulting in capillary bridges and meandering structures.
Experiments show that instabilities may also affect the
initial situation of a thermal nanoimprint process. Already
at the beginning of the actual imprint step, the polymeric
surface may be highly non-uniform, with undulations of the
film thickness, polymeric bridges and de-wetted regions;
thus, the starting point for imprint may differ substantially
from the general expectation of a uniform spin-coated
layer. A detailed instability analysis considering the com-
bined effect of van der Waals forces, electrostatic forces
and temperature gradients under realistic imprint condi-
tions clearly identifies temperature gradients to be the
cause for high initial layer non-uniformities. We found that
during heat-up (before imprint) temperature differences of
10 °C may exist between the top and bottom hotplate of a
thermal imprint system. These temperature differences
result in the non-uniformities of the polymeric layer
observed, when stamp and sample are heated under low-
pressure contact, where some small but locally arbitrary
gaps exist between polymer and stamp. This result asks for
a reconsideration of the thermal nanoimprint procedure. It
also confirms the high impact of temperature control for
uniform, low-defect imprint results; this is critical not only
during imprint, but also during heat-up.

✉ H.-C. Scheer
   scheer@uni-wuppertal.de

1   Microstructure Engineering, University of Wuppertal,
    Rainer-Gruenter-Str. 21, 42119 Wuppertal, Germany

1 Introduction

With nanoimprint, instabilities occurring in polymeric
layers are 'Janus-faced.' In most cases they result in
imprint defects, e.g., when the imprint is performed in thin
polymeric layers in order to achieve thin or negligible
residual layers [1]. However, instabilities have also been
proposed to define specific patterns in a polymeric layer
with only (partial) contact to the elevated stamp structures,
e.g., to shape regular pillar arrays (LISA, lithography-in-
duced self-assembly [2]) or to replicate stamp structures
with the same tone as the stamp, without inversion (LISC,
lithographically induced self-construction [3]).

For these reasons, instabilities have been studied in
detail experimentally [4–6] as well as theoretically [6–13].
They develop, when small gaps between the polymeric
surface and the stamp are present. The main drivers are van
der Waals forces [13], temperature gradients [10] and
electrostatic forces [7, 8] that are counteracted by capillary
forces (surface tension). The time scale for their formation
depends on the viscosity of the layer. With instabilities, the
structures forming become visible when incomplete
imprints are 'frozen-in,' either by cross-linking (UV-NIL,
UV-assisted nanoimprint) or by cooldown (T-NIL, thermal
nanoimprint). Due to the formation under physical inter-
action, the process is often termed 'physical self-assem-
bly.' In UV-NIL, physical self-assembly is highly
correlated with bubble trapping [14–16].

Figure 1 gives typical examples of patterns observed
with imprinted samples, resulting from instabilities [18].
Within large cavities that are not completely filled, capil-
lary bridges (Fig. 1a) may have developed locally and may
span gaps of more than a micron in height; with a some-
what higher filling level, the bridges merge and form
meandering structures (Fig. 1b); and within linear cavities,

Fig. 1 Typical examples for physical self-assembly during nanoimprint. Polymeric bridges within wide cavities at low filling level (**a**) and high filling level (**b**) in the stamp cavities; similar situation with wide line cavities, again at low (**c**) and high (**d**) filling level. With narrow line cavities, typically broken lines develop (**e**), with complete de-wetting of the polymer at the substrate at the defect locations (**f**)
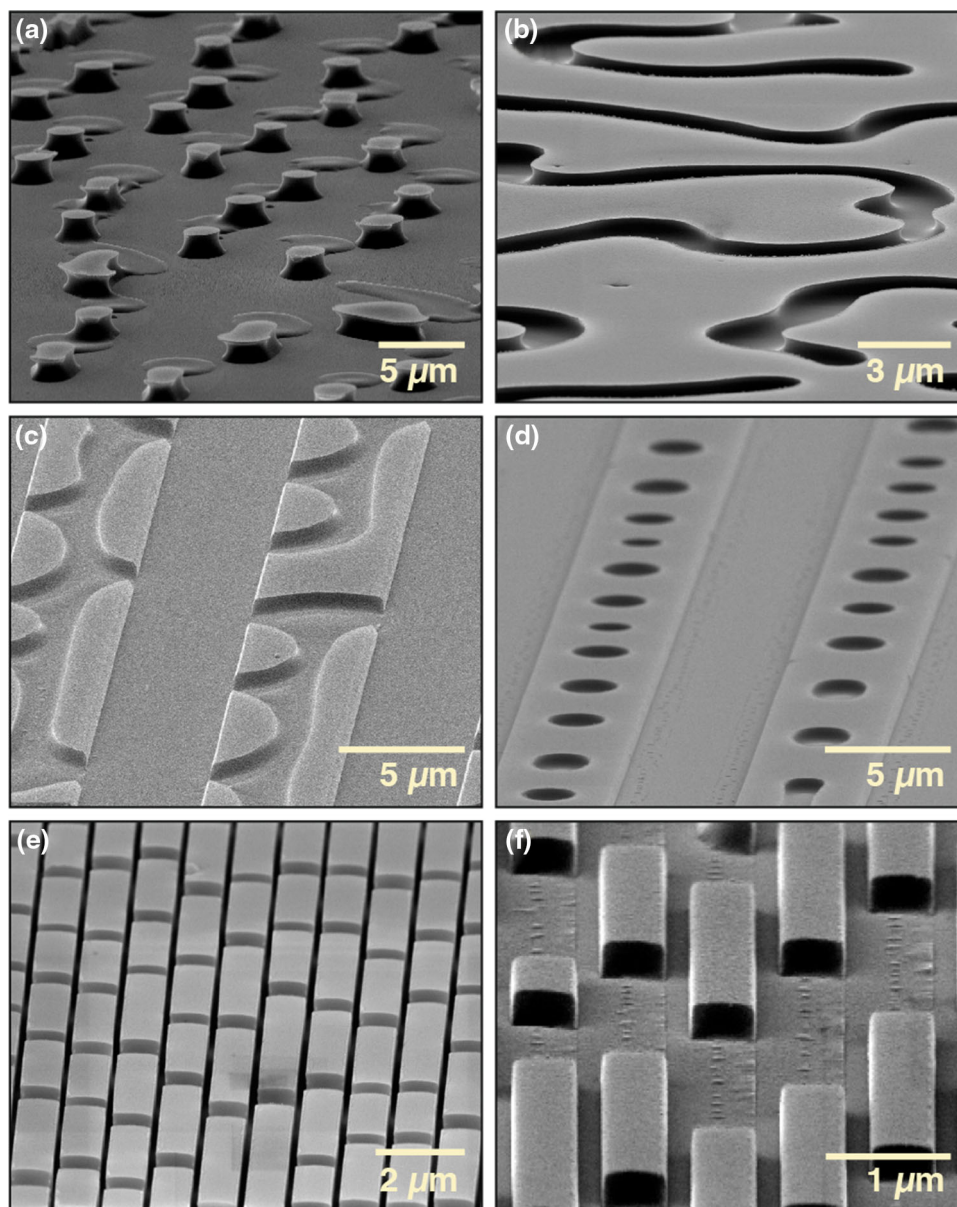
polymeric assembly is observed along the cavity edges (Fig. 1c) at low filling levels, developing into a necklace-like defective pattern along the cavity center at a higher filling level (Fig. 1d). With smaller geometries, the assembled polymer fills the whole width of the cavity and defects result in an almost regular on–off pattern along the lines (Fig. 1e), often with complete de-wetting of the polymer at the substrate in between the assembled regions (Fig. 1f). The results documented in Fig. 1 were obtained with polystyrene during T-NIL at 190 °C, with a polymer viscosity of about 10^4 Pas, within a typical imprint time of ≤5 min. Similar patterns are observed with other polymers at a comparable or even lower viscosity as reported by other groups. Furthermore, the occurrence of instabilities is

not restricted to T-NIL; such structures are also observed with UV-NIL and, for example, capillary force lithography (CFL) [17].

Although these instability-induced patterns are well known and are identified as defects when complete replication of the stamp structures is envisaged, the impact of instabilities with respect to a successful imprint may be much stronger than actually believed. This contribution addresses the impact of instabilities with respect to the 'initial condition' for an imprint, and the results obtained suggest the reconsideration of a generally accepted imprint procedure where heating up of the imprint stack is performed under low contact pressure to facilitate isothermal conditions.

2 Methodology of experiments

Thermal imprint experiments were performed in a laboratory imprint system [19] with polystyrene (PS, 350 kg/mol, Sigma-Aldrich). The layer thickness was 500 nm; the layers were baked for solvent removal (120 °C, 15 min, hotplate). Prior to spin-coating, the Si substrates were dehydration-baked (200 °C, 5 min, hotplate) to improve adhesion. The stamps used are positive ones (elevated structures, structure height 350 nm), almost completely patterned with line structures (widths 300 nm–3 μm) across the overall area of 1.5 cm × 2 cm. The stamps were provided with an anti-sticking layer from the gas phase. Stamps as well as substrates were cut from 100-mm-diameter Si wafers with a thickness of 500 μm.

In order to investigate the 'initial condition' for an imprint, T-NIL experiments were performed similar to a conventionally accepted imprint procedure, but by omitting the imprint step itself. Stamp and sample were heated to the imprint temperature (190 °C) under low-pressure contact (400 N) to assure isothermal conditions for the imprint. When the imprint temperature was reached after about 20 min, (rapid) cooldown (water shock-cooling) was initiated without applying any imprint pressure. Thus, the situation prevailing at the beginning of a typical imprint process was frozen-in. The results are documented by scanning electron microscopy (SEM) measurements.

3 Discussion of experimental results

Typical experimental results obtained after simple heat-up and cooldown, without applying the imprint pressure are shown in Fig. 2. When interpreting them, one has to bear in mind that under low-pressure contact during heating, a locally differing gap between stamp and substrate will exist, due to the limited flatness of all surfaces involved, the press plates as well as the Si substrate and stamp. The low pressure applied results in a local contact (which may even change due to thermal expansion of the components during heat-up), with gaps of locally varying width between the (structured) stamp surface and the surface of the polymeric layer on the substrate. Figure 2a shows a local capillary bridge of more than 1 μm in height, developed within a wide cavity of the stamp; the formation of the bridge resulted in a strong rearrangement of the polymeric layer around the bridge as suction effects toward the bridge have depleted the surrounding area, which is locally de-wetted. Even without complete bridge formation, the polymeric surface may look as if it were 'boiling' (Fig. 2b), with undulations in the micrometer range and heights of up to ≈500 nm. The surface undulations (and
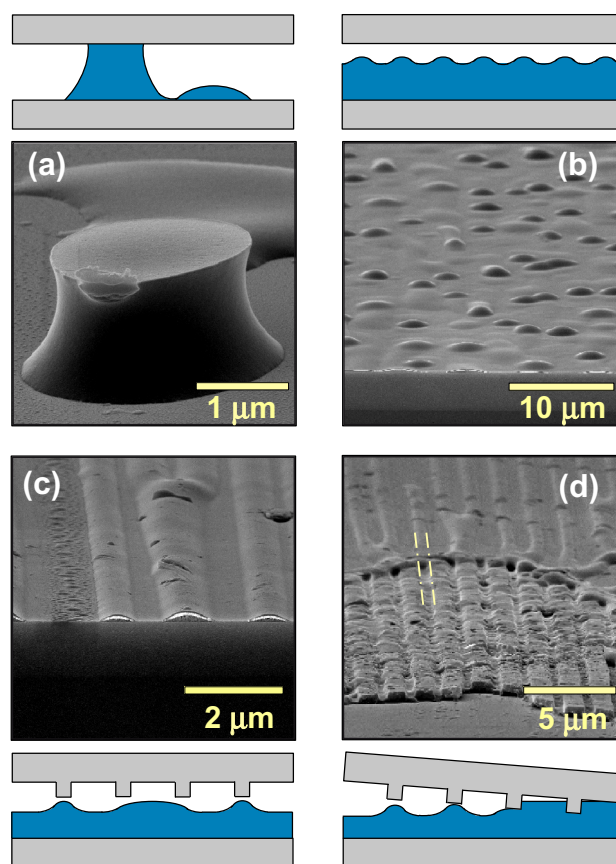

Fig. 2 Topographies obtained with a layer of PS when heated to the imprint temperature in low-pressure contact to a patterned stamp, followed directly by cooldown, without an imprint step. Each SEM micrograph is complemented by a sketch of the situation. **a** Polymeric bridge of more than 1 μm height, surrounded by a highly de-wetted region; **b** polymer surface looking as if boiling, the undulations representing the initial status of an instability formation in a wide cavity; **c** similar situation with a line structure in the stamp: The undulations are correlated with the stamp lines; **d** transition from a non-contact region (*top*) to a contact region (*bottom*) between polymer and stamp surface. In non-contact, the elevated lines guide the undulations, and in contact, the cavities dominate due to the action of capillary forces

bridges) observed have a periodicity in the range of some micrometers; they are a consequence of the interaction between the polymer and the stamp surface occurring during heat-up.

In locations where the stamp is patterned, the stamp topography results in a local modulation of the interaction forces and thus in guiding effects for the instabilities. Such a situation is shown in Fig. 2c, d, where the stamp features lines of 400 nm in width and a period of 1.6 μm. Though without any contact to the stamp protrusions, the linear undulations visible correspond to the elevated lines of the stamp, but their period is sometimes different (Fig. 2c, top part of SEM micrograph); one undulation may correspond to adjacent stamp protrusions; alternatively, due to local

suction, single protrusions are missing. The sketch corresponding to the SEM micrograph indicates this.

Figure 2d documents an even more complex situation, a transition from undulations (due to instabilities) to capillary filling. Obviously, the gap between stamp and sample increases slightly from the front to the back of the SEM image (in the sketch this is indicated from left to right). With a higher gap (top of SEM picture, left in the sketch), undulations are visible below almost each elevated line of the stamp. With a decreasing gap (bottom of SEM picture, right part of sketch), the undulations come into contact to the stamp surface and capillary forces drive the filling of the stamp cavities: All cavities are discernable in the lower part of the SEM picture; the cavities are only partially filled, as visible from the rough polymeric surface. The matching of the linear undulations with the elevated lines of the stamp is best documented at the left of Fig. 2d, where the undulation line continues as the (imprinted) elevated stamp line (see dash-dotted mark), with the partly filled cavities left and right of it.

These results document that already before the start of the actual imprint step, during heat-up, the polymeric surface has lost its flatness. Most critical may be a situation like the one shown in Fig. 2a, where the whole polymer has assembled in a high bridge, with no more polymer remaining in the area surrounding it. Thus, in a thermal imprint, where the heat-up is performed under low-pressure contact, a highly non-uniform layer thickness of the polymer may prevail at the beginning of the imprint, in contrast to what is expected generally, a uniform layer. This adds a further complication to the issue of volume conservation during imprint into spin-coated layers, a situation already suffering from non-uniformity due to pattern size effects [20, 21].

The results observed were obtained without an intentional temperature difference between stamp and sample and without any external field applied. Thus, electrostatic forces and temperature gradients are not expected as driving forces for instabilities; only van der Waals forces remain, which generally are expected to be low compared with the other two. Therefore, a detailed analysis of the theory of instabilities was performed in order to identify the reasons for the experimental results obtained.

4 Instability analysis

Our assessment is based on the general concept of a 'linear stability analysis' of thin films, the theory on this basis being provided by Schäffer [6, 7, 10, 11] and the classical analysis by Vrij [13]; but in contrast to Schäffer, who discussed the different driving forces separately, we combine them and apply them to a typical thermal imprint

situation, where the polymer is confined between the stamp surface and the substrate surface and the polymer–air interface either feels the interaction to the substrate or to the stamp, depending on the distance to the respective surface (and thus the strength of the respective combined interaction force). The analysis covers van der Waals forces, electrostatic forces as well as temperature gradients as driving forces for the instability.

Before combining the effect of all these forces under realistic imprint conditions, the three driving forces will be discussed separately and the principles of linear stability analysis are briefly reviewed, reduced to the main equations required for an understanding of the results.

4.1 Procedure with linear stability analysis

With stability analysis, a purely laminar flow of the polymer within a thin layer (in an x–y plane) is assumed, with the continuity equation (volume conservation, Poiseuille equation) relating the height h of the polymer layer to the pressure gradient within the layer—for simplicity reasons, we restrict our analysis to a planar problem (flow in x direction only, see Fig. 3). At the substrate, a vanishing velocity is prescribed (no-slip boundary), and at the free surface (polymer/air interface), the velocity is maximum.

The force per area that is effective across the polymer/air interface (where the maximum flow proceeds) is separated into two main components, a stabilizing component, p_{stab}, and a destabilizing component, p_{des}. The latter is composed of contributions from van der Waals forces as well as potential electrostatic forces and temperature gradients, $p_{des} = p_{vdW} + p_{el} + p_{\Delta T}$. The stabilizing
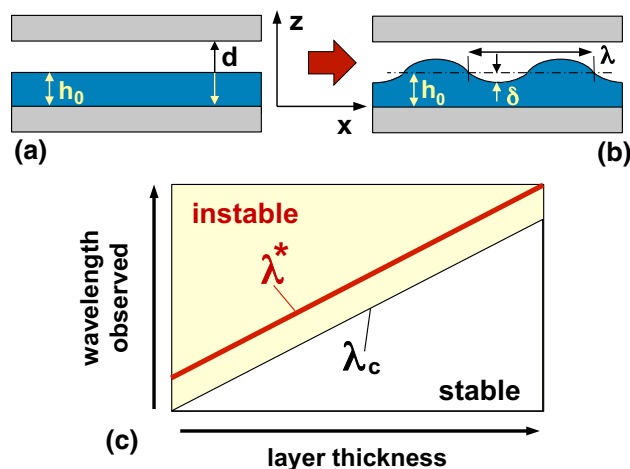

Fig. 3 Smooth polymeric layer (a) on a substrate with an air gap to the stamp (sketched without patterns here for simplicity) becomes unstable (b) and develops undulations (amplitude δ, wavelength λ) on its surface; stable and instable regions in the wavelength-layer thickness regime (c)

component always present is the Laplace pressure due to surface tensions with curved surfaces, $p_{stab} = \Delta p_{LA} = -\gamma\kappa$, with γ the surface tension of the polymer and κ the curvature of the surface, here $\kappa = d^2h/dx^2$. (The Laplace pressure is defined as the pressure difference between the pressure inside the liquid and the pressure in the adjacent gas phase, $\Delta p_{La} = p_{liquid} - p_{gas}$).

With these assumptions, the differential equation governing the temporal and spatial behavior of the layer height $h(x, t)$ is given by

$$\frac{\partial h(x, t)}{\partial t} = \frac{\partial}{\partial x}\left(\frac{h^3}{3\eta} \cdot \frac{\partial}{\partial x}(p_{stab} - p_{des})\right)$$
$$\approx \frac{h^3}{3\eta} \cdot \frac{\partial^2}{\partial x^2}\left(-\gamma\frac{\partial^2 h}{\partial x^2} - p_{des}\right) \quad (1)$$

The approximation refers to the linearity of the analysis, neglecting products of differential terms. (Due to the constant value of the gas pressure, the pressure change in the liquid reduces to the change of the Laplace pressure, $dp_{liquid}/dx = d(p_{gas} + p_{La})/dx = d\Delta p_{La}/dx$).

Now a small, stochastic undulation of the surface, δ, is assumed (see Fig. 3), in accordance with Eq. (1). Any local height modulation can be approximated by a series of periodic functions [13] (Fourier series), each of them having a different amplitude δ_i (with $\delta_i \ll 1$), time constant τ_i and periodicity as characterized by the respective wave number k_i. Finally, only one of these undulations is of interest; it is the one with the fastest growing amplitude. Only a growing amplitude (a positive time constant, $\tau_i > 0$) will result in an amplification of the small, stochastic undulation and thus may induce an instability in the film, the fastest growing one overriding all others, so that finally only this one survives (decreasing amplitudes ($\tau_i < 0$) do not lead to instabilities). With this single undulation, the time constant features a minimum, $\tau_{min} = \tau^*$; this minimum time constant is correlated with a single local periodicity as described by the wave number $k(\tau_{min}) = k^* = 2\pi/\lambda^*$, λ^* being the respective local wavelength.

The stability limit is given by $\tau_i = 0$, resulting in a critical wavelength $\lambda_C = \lambda^*\sqrt{2}$, as discussed in detail by Vrij [13]. Undulations with a wavelength $\lambda > \lambda_C$ grow in amplitude and thus result in instabilities, undulations with wavelengths $\lambda < \lambda_C$ decay, and the layer remains stable. Thus, curves $\lambda^*(h_0)$ as given below are within the instable regime, although only a factor of $\sqrt{2}$ away from the stability–instability transition. A general picture of the regimes and their boundary defined by λ_C is sketched in Fig. 3c.

For simplicity, only the equations for a single undulation are given here. The undulated polymer height is described as

$$h(x, t) = h_0(1 + \delta \cdot exp(jkx + t/\tau)), \quad (2)$$

resulting in a characteristic equation of

$$\frac{1}{\tau} = \frac{h_0^3}{3\eta} \cdot \left(\gamma k^4 + \frac{\partial p_{des}}{\partial h}k^2\right), \quad (3)$$

that correlates the growth rate $1/\tau$ with the mean height h_0 (the initial layer height of the polymer), its surface tension γ, its viscosity η at the imprint temperature and the change of the destabilizing pressure p_{des} with h. (In deriving Eq. (3) from an insertion of Eq. (2) into Eq. (1), all changes of the thickness that are not linear were neglected, in accordance with 'linear stability analysis').

The maximum growth rate is obtained for

$$(k^*)^2 = \left(\frac{2\pi}{\lambda^*}\right)^2 = -\frac{1}{2\gamma} \cdot \frac{\partial p_{des}}{\partial h}\bigg|_{h=h_0} \quad (4)$$

Thus, the final wavelength visible in an experiment, λ^* (the 'most unstable wavelength'), depends on the surface tension only, whereas the time constant also involves the viscosity. Any 'real' surface undulation requires a negative change of the respective destabilizing pressure with layer thickness, $dp_{des}/dh < 0$. For the calculations, values typical of PS at the imprint temperature were used, $\gamma(190\ °C) = 31$ mN/m and $\eta(190\ °C) = 10^4$ Pas.

In the following, the most unstable wavelength λ^* is given as a function of the initial layer thickness h_0. The destabilizing pressure is given by the sum of all potential contributions, the van der Waals forces (p_{vdW}), the electrostatic forces (p_{el}) and the temperature gradients ($p_{\Delta T}$). Before discussing the combined effect of all destabilizing pressures, each component is addressed separately.

4.2 van der Waals forces

The result obtained with van der Waals forces is summarized in Fig. 4. For calculation, an imprint situation as sketched in Fig. 4a is assumed. The interactions between polymer and substrate as well as between polymer and stamp are considered, different from the approach of Schäffer [6] involving polymer–substrate interaction, only. According to our knowledge of the literature, this is novel. The imprint stack is shown in Fig. 4a, the polymer on the substrate with an air gap to the stamp (left) or, in more detail, including the native oxide ($s_{nOx} = 1$ nm) of the Si stamp and the Si substrate (similar to Seemann [22]) as well as the anti-sticking layer ($s_{ASL} = 1$ nm) of the stamp (right). To the best of our knowledge, such realistic conditions have never been considered before by other groups. The van der Waals interactions across the polymer layer (indicated as p_{pol} in Fig. 4a) and across the air gap (indicated as p_{air} in Fig. 4a) are given by [23]
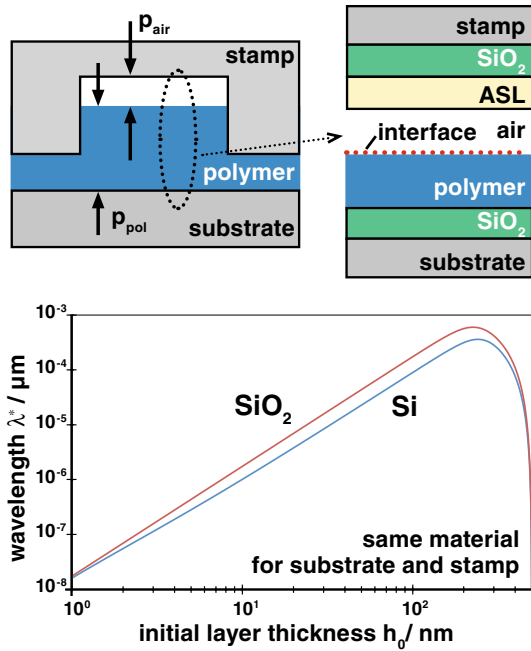
Fig. 4 Impact of van der Waals forces with instabilities. **a** Sketch of the respective situation; within the cavity, the stack is composed of seven layers, contributing to the van der Waals forces. **b** Most unstable wavelength as a function of the mean layer thickness, calculated for two different materials, Si and SiO$_2$

$$p_{pol} = -\frac{1}{6\pi}\left(\frac{A_1}{h_0^3} + \frac{A_2}{(h_0 + s)^3}\right) + C_1 \tag{5a}$$

$$p_{air} = +\frac{1}{6\pi}\left(\frac{A_3}{(d - h_0)^3} + \frac{A_4}{(d - h_0 + s)^3} + \frac{A_5}{(d - h_0 + 2s)^3}\right) + C_2,$$
$$p_{vdW} = p_{pol} - p_{air}, \tag{5b}$$

with h the polymer height, d the gap between stamp and substrate surface and $s = s_{nOx} = s_{ASL}$ the thicknesses of the native oxide and the anti-sticking layer, respectively. Interactions that remain constant when the polymer height changes are indicated by the additional constants C_1 and C_2—they do not enter Eq. (4). For an estimation of the respective Hamaker constants (A_i), we followed the approach of Israelachvilii [23, 24] based on image forces (see Table 1). Data for the dielectric constants (required for calculation of A_i) were taken from the literature [23].

The most unstable wavelength $\lambda*$ as a function of the initial layer thickness for a stamp cavity height of 500 nm is given in Fig. 4b; in addition to Si as the material for stamp and substrate (as most often used in T-NIL) also a curve for SiO$_2$ (as used, e.g., in UV-NIL) is given. With thin layers, the interaction of the polymer with the substrate is most prominent, increasing thicknesses resulting in an increase in the wavelength observed. The exponent n for the wavelength dependence ($\lambda* \sim h_0^n$) is in accordance

with classical results obtained by Vrij [13] and also with the results obtained by Schäffer [6]. As expected, with thin layers there is no more difference between Si and SiO$_2$ as the stamp material. This part of the curve, related to the substrate–polymer interaction, is responsible for the de-wetting of the polymer at the substrate, as discussed in detail with stability issues of thin films in general [25].

With thick layers (small air gap in the stamp cavity), $\lambda*$ decreases again, as the interaction between polymer and stamp surface is most prominent now. (The asymmetry of the curves results from the logarithmic scaling and the presentation as a function of the initial layer height. A logarithmic presentation as a function of the gap height ($H-h_0$) would show the opposite asymmetry).

4.3 Electrostatic forces

In order to calculate the impact of electrostatic forces (Fig. 5), the same correlations for p_{el} were used as in the literature [6, 7]. The force per area acting on the polymer/air interface is

$$p_{el} = -\varepsilon_0\varepsilon_{pol}(\varepsilon_{pol} - 1)\frac{U^2}{(\varepsilon_{pol}h + (d - h_0))^2} \tag{6}$$

The force per area of electrostatic interaction is independent from the polarization direction ($\sim U^2$) and thus always negative. As a consequence, any electrostatic interaction will result in a destabilization.

Strong interactions induced by electrostatic forces require the application of a voltage between the stamp and the polymer. This is possible, but it does not represent a conventional T-NIL situation. Conventionally, the stamp and the substrate are clamped together in the imprint system; thus, they are at almost similar potential. Nonetheless, a potential difference may exist across the imprint stack, and this is due to potential differences in the work function of the materials used for the stamp and the substrate, quite similar to the work function difference resulting in band bending at the surface of a field-effect transistor. The situation is sketched in Fig. 5b. With Si as both, the stamp and the substrate material, differing doping levels result in a potential difference, but this potential difference will be well below the energy corresponding to the band gap of Si. We assumed voltages of ≤ 1 V to calculate this case. With a metal stamp and a p-doped Si substrate, somewhat higher voltages may develop; we assumed voltages of ≤ 10 V to consider this case. The assumption of 100 V clearly refers to an externally applied voltage.

Results for the most unstable wavelength are given in Fig. 5a for the three voltage levels. Only with high initial layers (low gaps to the stamp) the electrostatic interaction results in a distinct decrease in $\lambda*$ and thus in a stability limitation. This is due to the fact that the interaction

Table 1 Hamaker constants calculated according to the image force method [22, 23] from dielectric constants (Si: 11.6; oxide: 3.8, polymer (PS): 2.55; ASL: ≈ 3.8)

Interacting interfaces	Hamaker constants
Polymer/air–polymer/native oxide of substrate	$A_1 = -4.88 \times 10^{-20}$ J
Polymer/air–Si substrate	$A_2 = -14.84 \times 10^{-20}$ J
Polymer/air–ASL/air	$A_3 = 13.6 \times 10^{-20}$ J
Polymer/air–ASL/native oxide of stamp	$A_4 \approx 0 \times 10^{-20}$ J
Polymer/air–Si stamp	$A_5 = 14.84 \times 10^{-20}$ J

The value obtained for A_4 is negligible with our samples, due to the negligible difference in dielectric constants at the ASL/native oxide interface; we determined the ASL data for our samples from spectroscopic ellipsometry measurements
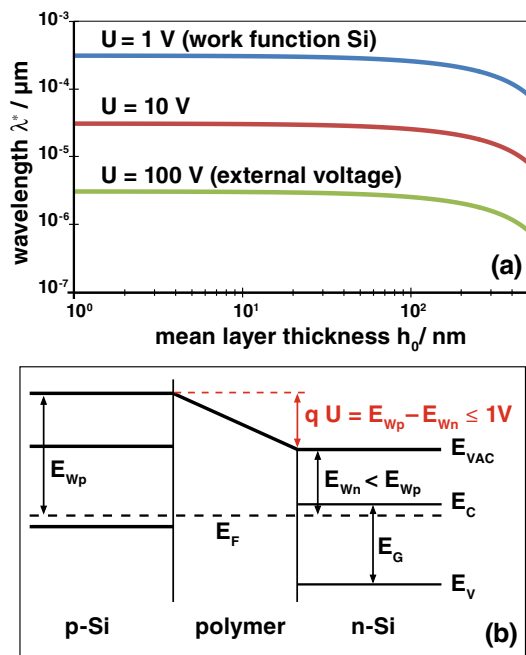

Fig. 5 Impact of electrostatic forces with instabilities. **a** Most unstable wavelength as a function of the mean layer thickness, calculated for three different potential differences. **b** Sketch of respective situation without an externally applied voltage; between the Si stamp and the Si substrate, a potential difference of ≤1 V may exist due to differences of the work function E_W of the materials involved

Fig. 6 Impact of temperature gradients with instabilities. **a** Most unstable wavelength as a function of the mean layer thickness, calculated for two different temperature gradients. **b** Measured temperatures of the *top* and *bottom* hotplate in a typical imprint system. Temperature differences of $\Delta T_2 = 10$ V were recorded during heat-up; during imprint the temperature difference is lower, $\Delta T_1 = 1$ V

between polymer and stamp across the air gap (where the electric field is higher than in the polymer) increases inversely proportional to the gap height. The higher the voltages acting, the lower the limiting values λ^*.

4.4 Temperature gradients

For an estimation of the impact of temperature gradients (Fig. 6), again the equation given by Schäffer [10] for $p_{\Delta T}$ was used, together with his estimated values for the sound velocity. The force per area is denoted by
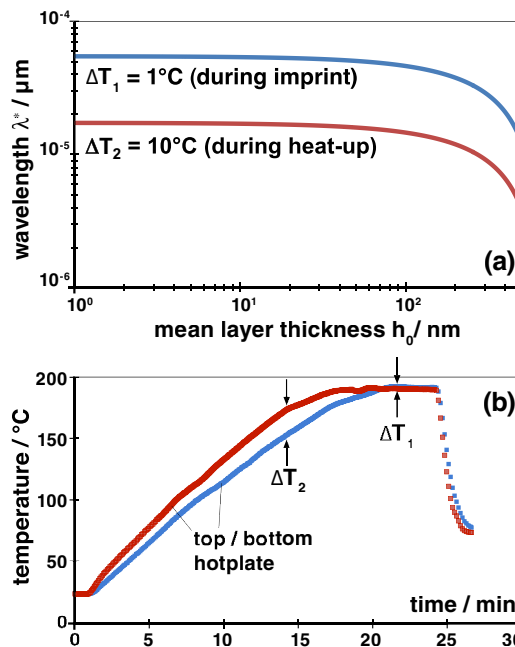
$$p_{\Delta T} = -\frac{2\kappa_{air}\kappa_{pol}}{u_{eff}} \frac{\Delta T}{\kappa_{air}h + \kappa_{pol}(d - h_0)},$$

with κ_{air} and κ_{pol} the thermal conductivities and u_{eff} the effective sound velocity in the polymer on a Si substrate. (Parameters [10]: $\kappa_{air} = 0.034$ W/Km; $\kappa_{pol} = 0.16$ W/Km; $u_{eff} = 265$ m/s).

We only assumed a certain temperature gradient between stamp and substrate to calculate the respective effect. As we did not intentionally provide any temperature difference between stamp and substrate (most often T-NIL is performed as an isothermal process), we measured the temperature profiles of the lower and upper hotplate of a

typical imprint system during heat-up. The respective curves are given in Fig. 6b. We found that temperature differences of up to 10 °C may temporarily exist during heat-up, before an isothermal state is reached (where in general the imprint is performed). Such a difference may result from differing thermal loads in direct contact to the hotplates, using parts of the heating energy supplied in being heated up. Thus, we assumed a maximum temperature difference of 10 °C. In order to have a lower limit, too, we assumed a temperature difference of 1 °C, which may result from independent (non-correlated) control of the temperature of both press plates.

The respective result is shown in Fig. 6a. Similar to the electrostatic case, the curves decrease with high layer thickness (low gap) only, and only distinct temperature differences limit the stability.

4.5 Combined effect

Figure 7 gives the most instable wavelength as a function of the initial layer thickness, when all destabilizing forces act in parallel. The gap height assumed is again 500 nm. Figure 7a, b assumes a maximum temperature difference of 1 and 10 °C, respectively and gives results for the three different voltages taken as an example, 1, 10 and 100 V. The combined curves are dominated by van der Waals forces with small layer thickness ($h_0 < 50$ nm) as well as
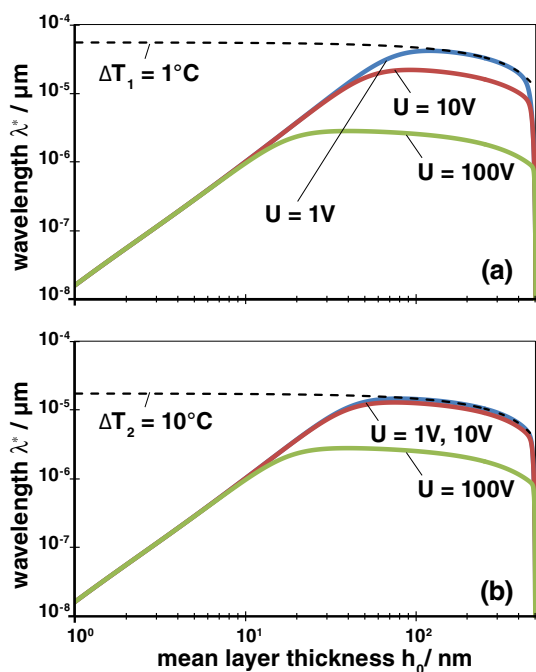

Fig. 7 Most unstable wavelength as a function of mean layer thickness under the combined effect of all forces. **a** Low temperature gradient (1 °C), **b** increased temperature gradient (10 °C); voltage levels similar as Fig. 4

with small gap height (gap $(d-h_0) < 50$ nm). The center region ($50 < h_0 < 450$ nm) is dominated by temperature gradients and electrostatic forces. The temperature difference defines some upper limit (see dashed line): with $\Delta T = 1$ °C, potential differences of some volts are already effective to further limit the most unstable wavelength and with $\Delta T = 10$ °C, some 10 V are required to become effective. Roughly, at low temperature differences the intermediate range is dominated by electrostatic forces, but at high temperature difference the temperature gradient predominates the electrostatic forces, in particular without an external voltage applied. The limiting character of the temperature gradient becomes clear-cut when comparing Fig. 7a and b: The curve for $U = 10$ V is decreased in Fig. 7b compared with that in Fig. 7a.

Within the center regime, the curves are almost flat (the most unstable wavelength is almost the same for a wide range of mean layer thickness values); thus, it is not possible to derive an indication for the cause of the instability (whether it is induced by a temperature gradient or by an electrostatic interaction) from a characteristic change of the wavelength with the layer thickness.

In our system, with temperature differences up to 10 °C during heating and without intentionally applied voltage ($U \leq 1$ V), undulations with a wavelength around 10 μm have to be expected, almost across the whole range of initial (mean) layer thickness. This corresponds to our experience (see Fig. 1, 2).

Finally, Fig. 8a gives the maximum growth rate for three different viscosities—the value of 10^4 Pas is typical of our imprint polymer PS at a temperature of 190 °C. Again a temperature difference of 10 °C was assumed and a voltage difference of 1 V, similar to the conditions in our experiment. As expected, the maximum growth rate decreases with increasing viscosity (Eq. 3). For a typical imprint situation with total times of an imprint cycle (heating, imprint, cooldown) in the range of 10–15 min at elevated temperature (above the glass transition), a growth rate of about 10^{-3} s^{-1} (see horizontal line in Fig. 8, referring to $t/\tau = 1$) becomes critical. A small undulation of the polymer height may be amplified, so that the top of the stamp cavity is reached and a bridge forms. With the different viscosities assumed, an initial mean layer thickness above about 200, 300 and 400 nm may result in physical self-assembly for viscosities of 10^4, 10^5 and 10^6 Pas, respectively (see * in Fig. 8a). This is in agreement with the finding that a reduced imprint temperature reduces the defect density.

Figure 8b shows the situation with different gap heights, 0.5, 1 and 1.5 μm; again, by valuating the curves with respect to the critical growth rate (10^{-3} s^{-1}), the accepted knowledge is confirmed, a high gap reduces the risk of self-assembly. As indicated in the figure, a relative filling level
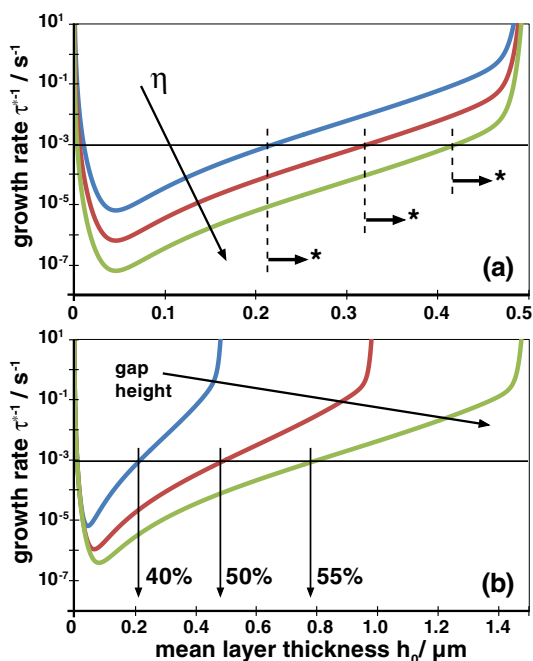
Fig. 8 Maximum growth rate as a function of mean layer thickness under the combined effect of all forces; the temperature gradient assumed is 10 °C. **a** Effect of different viscosities (10^4, 10^5 and 10^6 Pas) of the polymer. **b** Effect of different gap heights (0.5, 1 and 1.5 μm) at $\Delta T = 10$ °C and a viscosity of 10^4 Pas. The *horizontal line* refers to an imprint time (15 min) equal to the time constant t^*

above 40, 50 and 55 % would result in self-assembly with gaps of 0.5, 1 and 1.5 μm, respectively.

Furthermore, Fig. 8b is able to explain our experiments in Fig. 2c, d. With a certain initial layer thickness, the growth rate is more than one decade higher with a gap of, for example, 1 μm than with a gap of 1.5 μm. Therefore, self-assembly is formed below the elevated stamp structures first, as shown in Fig. 2c. Without stamp topography, the most unstable wavelength is dictated by λ^* as calculated; with a stamp topography featuring a differing period p, the local force modulation results in a compromise; in parts the surface undulations follow λ^*, in parts they follow the stamp period p, as visible in Fig. 2c, d.

In view of the initial situation for imprint, as primarily addressed here, we have to state that the temperature difference during heat-up is the most critical issue with our process. With our temperature difference of 10 °C, the most unstable wavelength is about 10 μm, in full agreement with our experiments (Fig. 1, 2).

4.6 Consequences

Without an externally applied electric field, temperature gradients are by far most critical with respect to the formation of instabilities. The measurements obtained in our laboratory system (as documented in Fig. 6a), where a temperature difference of 10 °C was measured during heat-up, are not unrealistic. With commercial imprint systems, even higher temperature differences were found, during heat-up and also during cooldown (up to 35 °C), and even during the imprint step (full pressure applied), temperature differences of up to 5 °C were measured.

To avoid instabilities during heat-up and thus to maintain a uniform initial polymer layer before the imprint starts, the gap between stamp and polymer has to be controlled, as documented in Fig. 8b. Temperature differences during heat-up are only critical when low-pressure contact is provided during heating—with a high gap (e.g., realized by spacers between the stamp and the substrate), instabilities are not provoked and the initial film thickness remains uniform, as spin-coated.

Temperature differences during imprint are critical as well, as there exists a small gap within the stamp cavities that are not yet completely filled—there the structures typical of physical self-assembly (see Fig. 1) will develop. With long cooling times (no shock-cooling), temperature differences also become critical during cooling, as the polymer still has a low viscosity at temperatures above the glass transition, and again a small gap may exist in the stamp cavities due to the high pressure still applied during cooldown, when typical imprint procedures are followed.

The calculations show that temperature control is most critical with T-NIL; in particular, temperature differences between top and bottom hotplate (stamp and substrate) have ultimately to be avoided. This refers not only to the actual imprint step, but also to the heating and cooling step. Instabilities may form already during heat-up, before the imprint, resulting in a highly non-uniform initial layer, as already stated experimentally by Chaix [4]. We think that these results suggest a reconsideration of the setup used for thermal imprint, or a reconsideration of the imprint procedures followed.

5 Summary

Experiments were performed to characterize the heat-up phase during thermal imprint, where a low-pressure contact is installed in order to assure isothermal conditions. As soon as the imprint temperature was reached, cooldown was initiated, without any imprint phase under elevated pressure. The experiments revealed a highly non-uniform surface of the polymer, instead of the conventionally assumed uniform thickness of the spin-coated layer. Such a non-uniformity has ultimately to be avoided in order not to affect the uniformity of the imprint, beyond the one resulting from pattern density differences in the stamp.

In order to understand the effects, a linear stability analysis was performed, considering the interplay of the Laplace pressure on the one hand and destabilizing forces due to van der Waals interaction, electrostatic interaction or temperature gradients on the other hand. The analysis clearly shows that without an externally applied voltage any temperature difference between stamp and polymer during heat-up or imprint is crucial. We could identify a temperature gradient of about 10 °C occurring during heat-up in our imprint system to be the reason for the effects observed. As a consequence, temperature differences between stamp and sample are most critical and have to be avoided; problems during heat-up should be minimized by holding a distinct gap between stamp and substrate instead of assembling the imprint stack without spacers and heating under low-pressure contact; alternatively, heating-up has to proceed under a high pre-pressure that is already sufficient to close any gap existing between polymer and stamp due to the wavyness of all surfaces involved.

References

1. N. Bogdanski, M. Wissen, S. Möllenbeck, H.-C. Scheer, J. Vac. Sci. Technol. B **24**, 2998–3001 (2006)
2. P. Deshpande, X. Sun, S.Y. Chou, Appl. Phys. Lett. **79**, 1688–1690 (2001)
3. S.Y. Chou, L. Zhuang, L. Guo, Appl. Phys. Lett. **75**, 1004–1006 (1999)
4. N. Chaix, C. Gourgon, S. Landis, C. Perret, M. Fink, F. Reuther, D. Mercerreyes, Nanotechnology **17**, 4082 (2006)
5. N. Chaix, S. Landis, D. Hermelin, T. Leveder, C. Perret, V. Delaye, C. Gourgon, J. Vac. Sci. Technol. B **24**, 3011–3015 (2006)
6. E. Schäffer, PhD Thesis, Konstanz, Germany, 2001
7. E. Schäffer, T. Thurn-Albrecht, T.P. Russell, U. Steiner, Nature **403**, 874–877 (2000)
8. Z. Suo, J. Liang, Appl. Phys. Lett. **78**, 3971–3973 (2001)
9. L. Wu, S.Y. Chou, Appl. Phys. Lett. **82**, 3200–3202 (2003)
10. E. Schäffer, S. Harkema, M. Roderdink, R. Blossey, U. Steiner, Adv. Mater. **15**, 514–517 (2003)
11. E. Schäffer, U. Steiner, Eur. Phys. J. E **8**, 347–351 (2002)
12. A. Vrij, 23. Disc. Farad. Soc. **42**(1966), 23 (1966)
13. A. Vrij, J. Colloid Sci **19**, 1 (1964)
14. H. Hiroshima, M. Komuro, N. Kasahara, Y. Kurashima, J. Taniguchi, Jpn. J. Appl. Phys. **42**, 3849–3853 (2003)
15. X. Liang, H. Tan, Z. Fu, S.Y. Chou, Nanotechnology **18**, 025303 (2007)
16. D. Morihara, H. Hiroshima, Y. Hirai, Microelectron. Eng. **86**, 684–687 (2009)
17. K.Y. Suh, H.H. Lee, Adv. Funct. Mater. **12**, 405–413 (2002)
18. A. Mayer, K. Dhima, S. Möllenbec, S. Wang, H.C. Scheer, J. Sakamoto, H. Kawata, Y. Hirai, J. Vac. Sci. Technol. B **30**, 06FB03 (2012)
19. A. Mayer, S. Möllenbeck, K. Dhima, S. Wang, H.C. Scheer, J. Vac. Sci. Technol. B **29**, 06FC13 (2011)
20. C. Gourgon, C. Perret, G. Micouin, F. Lazzarino, J.H. Tortai, O. Joubert, J.-P.E. Grollier, J. Vac. Sci Technol. **B21**, 98–105 (2003)
21. H. Schulz, M. Wissen, H.-C. Scheer, Microelectron. Eng. **67–68**, 657–663 (2003)
22. R. Seemann, S. Herminghaus, K. Jacobs, Phys. Rev. Lett. **86**, 5534–5537 (2001)
23. J.N. Israelachvili, *Intermolecular and Surface Forces* (Academic Press, Amsterdam, 2011)
24. J.N. Israelachvili, Proc. R. Soc. Lond. A **331**, 39–55 (1972)
25. G. Reiter, Phys. Rev. Lett. **87**, 186101 (2001)